Carbon structures in silicon carbide derived carbon

Sascha Welz [a,1], Michael J. McNallan [a], Yury Gogotsi [b,*]

[a] *University of Illinois at Chicago, Department of Civil and Material Engineering, 842 West Taylor St., Chicago, IL 60607, USA*
[b] *Drexel University, Department of Materials Science and Engineering, Philadelphia, PA 19104, USA*

Abstract

Carbide derived carbon (CDC) produced by etching SiC in halogens has been investigated using transmission electron microscopy (TEM). Depending on experimental conditions, CDC may contain sp^3- or sp^2-bonded carbon phases. Amorphous carbon, poorly ordered turbostratic carbon with lattice spacing exceeding values of 0.35 nm as well as highly ordered graphite were observed. sp^3-Bonded structures consist of mainly lonsdaleite and cubic diamond nanocrystals. Hexagonal diamond polytypes and n-diamond have been synthesized. During the annealing process, diamond nanocrystals eventually transform to sp^2-bonded carbons. The transformation process of hexagonal diamond nanocrystals produces spherical onion type structures. These structures appear either hollow or dense. The latter shows a decrease in lattice spacing compared to *d/n* values for graphite. Graphitic structures include multi-wall nanotubes, polyhedral particles and ribbons. The graphitization during chlorination of samples may eventually lead to the formation of planar graphite.
© 2006 Elsevier B.V. All rights reserved.

Keywords: Carbide derived carbon; Silicon carbide; Carbon; Transmission electron microscopy; Nanopores

1. Introduction

Selective etching of carbides in halogens is an attractive technique to produce carbon coatings that may include a variety of structures depending on the process parameters. Carbon produced by this process is known as carbide derived carbon (CDC) [1,2]. Its synthesis enables the formation of a variety of different carbon structures, including diamond, depending on experimental conditions. CDC can be produced as chlorine or HCl react selectively with the silicon at the SiC surface since $SiCl_4$ is thermodynamically more stable than CCl_4 [2]:

$$SiC + 2Cl_2 = SiCl_4 + C \tag{1}$$

$$SiC + 4HCl = SiCl_4 + C + 2H_2 \tag{2}$$
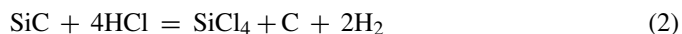
The main difference between the CDC process and other processes to produce carbon films is that the carbon is not deposited onto the surface of the substrate as in chemical and physical vapor deposition (CVD and PVD, respectively), but the surface of the carbide is converted to carbon. Owing to the conversion of

the surface, the dimensions of the initial untreated carbide particle remain unchanged, while other processes apply a carbon coating on top of the carbide thus increasing the size. Structural properties range from soft and porous to ultra hard. Nanoporous, amorphous carbons found in the film allow easy permeation of Cl_2, HCl, H_2, $SiCl_4$ and other gas molecules to the surface. Another indication for nanoporosity can be found by paying attention to the growth kinetics, which are linear in thickness with time. The most common carbon phase is planar graphite forming primarily a hexagonal structure. The other, less common structure is rhombohedral graphite. In addition to graphite, sp^2-bonded carbon in form of onions, ribbons, nanotubes and fullerenes can be synthesized. The formation of enclosed structures eliminates the dangling bonds and thereby reduces the total energy of the carbon atoms in the structure [3].

Literature reports, that cubic diamond is more stable than hexagonal diamond [4]. It is believed that the hexagonal structure possesses a slightly higher energy than the cubic diamond configuration because of the eclipsing sp^3-bonds along the tetrahedral apexes, which is similar to cyclohexane linkages. In hexagonal diamond, C–C bonds of one direction are rotated by 60° compared to cubic diamond. Thus, close packed layers (1 0 0) for hexagonal and (1 1 1) for cubic diamond, are equivalent but differ in their stacking sequence. These two types are considered to be the parent diamond structures because any other diamond polytypes are based on combination of layer sequences of 2H or 3C diamond. Other diamond polytypes such

* Corresponding author. Tel.: +1 215 895 6446; fax: +1 215 895 1934.
E-mail address: Gogotsi@drexel.edu (Y. Gogotsi).

[1] Present address: Department of Chemical Engineering and Materials Science, University of California at Davis and National Center for Electron Microscopy, MS 72-150, Lawrence Berkeley National Laboratory, Berkeley, CA 94720, USA.

as hexagonal 4H, 6H, 8H and 10H and rhombohedral 15R and 21R diamond phases have been theoretically predicted [5,6] and some of them experimentally confirmed (4H, 6H and 8H [7–9] 9R and 15R [10,11]).

To complete the group of known diamond polytypes, the so-called n-diamond belonging to the $F\bar{4}3m$ space group, has been reported [12,13]. Although other sp^3-bonded carbon structures are energetically less favorable with respect to 2C and 2H diamond, polytypism in diamond is possible and similar to SiC. It may be described as one-dimensional polymorphism produced by close packed diamond lattices.

The extraction of metals from carbides enables the synthesis of a variety of carbon structures such as amorphous carbon [2] to carbon onions [14] and diamond [1]. Although many papers have been published on properties of CDC and many different CDCs derived from different carbides have been reported [15], no systematic TEM study of carbon allotropes present in CDC has been published. This paper focuses on the identification of carbon structures in CDC using TEM techniques.

2. Experimental

2.1. Synthesis

Carbides used for CDC synthesis were α-SiC and β-SiC. α-SiC ceramics contained a mixture of polytypes, predominantly hexagonal 6H polytype, and were produced by Saint-Gobain and Elektroschmelzwerk Kempten (ESK). The β-SiC (3C polytype) powder with particle size of about 1 μm was produced by Superior Graphite Co., Chicago, IL. CDC was formed by placing the carbides in a fused silica tube furnace, exposing them to a flowing halogen gas mixture at atmospheric pressure and temperatures between 600 and 1000 °C [2]. The gas mixtures contained 3.5% Cl_2, 0–2% H_2 and balance Ar, which is used as an inert carrier gas. Experiments were performed on six different samples (Table 1).

2.2. Analysis

Carbon phases were identified using high-resolution transmission electron microscopy (HRTEM) (JEOL JEM-2010F, 200 kV and JEOL JEM-3010, 300 kV), energy dispersive X-ray spectroscopy (EDS), selected area electron diffraction (SAED), convergent beam electron diffraction (CBED) and electron energy loss spectroscopy (EELS). TEM imaging, SAED, CBED and lattice fringing measurements were performed on over multiple locations to accumulate statistically reliable experimental data. Gold was used for calibration of the TEM and electron transparent graphite flakes were attached to each of the TEM sample grids to assure accuracy in measurements of lattice spacing. The samples were prepared using conventional TEM sample preparation methods. CDC powders were ultrasonically dispersed in acetone and placed onto a supporting copper grid with a lacy carbon film. For interface studies, two rectangular pieces of CDC coated bulk material were cut to fit a TEM Cu washer. The pieces were mechanically polished and further thinned by ion milling using an Ar gas plasma in a GATAN ion mill to obtain an electron transparent interface.

Table 1
Samples and the process parameters used in this study

Sample	Gas mixture	Time (h)	Temperature (°C)	Consistency
S1	Cl_2	27	600	Powder
S2	Cl_2:H_2 = 2:0.75	24	1000	Powder
S3	Cl_2:H_2 = 2:0.5	20	1000	Powder
S4	Cl_2:H_2 = 2:0.5	24	1000	Bulk
S5	Cl_2:H_2 = 2:0.75	30	1000	Bulk
S6	Cl_2	24	1000	Bulk

3. Results

3.1. Amorphous and graphitic carbons

The material produced by pure chlorine gas treatment appears predominantly disordered and porous. Amorphous carbon is observed in samples treated at lower reaction temperatures between 500 and 600 °C (Fig. 1a). This is in agreement with previous observations [2]. Amorphous carbon is found throughout CDC and to a higher extent in the outer layers. It is in particular formed from SiC powders. Owing to the higher surface area of the powder, the reactivity is higher. As a result, the carbide converts faster to CDC producing an amorphous and disordered structure (sample 1). Its appearance is similar to amorphous carbons produced from bulk SiC at longer treatment times. CDC derived from β-SiC has a surface area exceeding 1000 m^2/g [2]. The temperatures of ∼600 °C during the CDC synthesis at ambient pressure are not sufficient to enable graphitization of these porous carbons even after 27 h. Amorphous carbon has also been found to have fullerenic nature with non-planar carbon structures including pentagonal and heptagonal rings (Fig. 1b) and formation of non-spherical closed and open shells is observed similar to ones described in [16,17]. Porosity in CDC enables reaction products such as $SiCl_4$ (1) to be transported to the surface. The values for porosity of diverse CDC treated carbides range from 53.6% for cubic VC to 83.1% for cubic Cr_4C [15]. The porosity for β-SiC derived CDC has been estimated as 57.2%. A two-dimensional schematic in Fig. 2 shows how porous carbon is
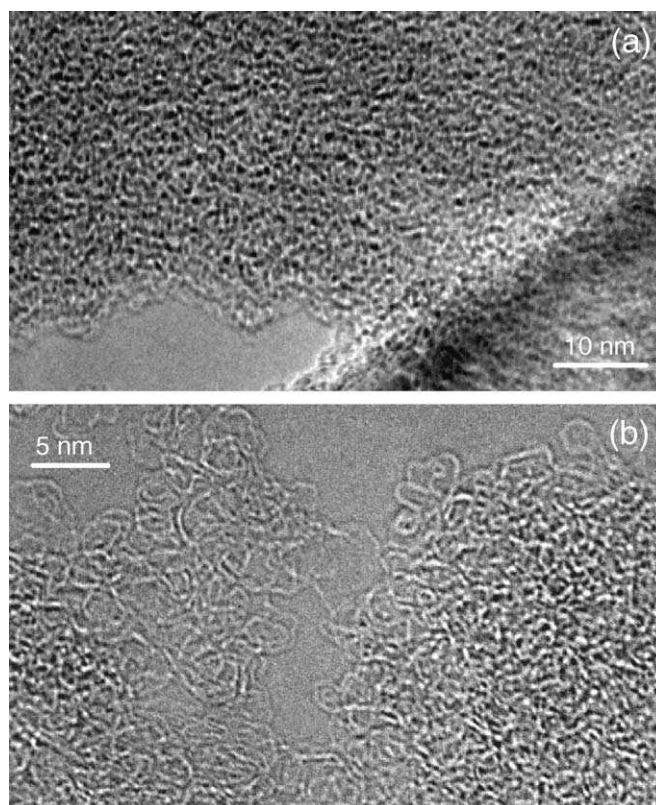

Fig. 1. (a) TEM image of a porous carbon structure found in the outer layer of CDC films (sample 1). (b) Carbon having fullerenic structure (sample 2).
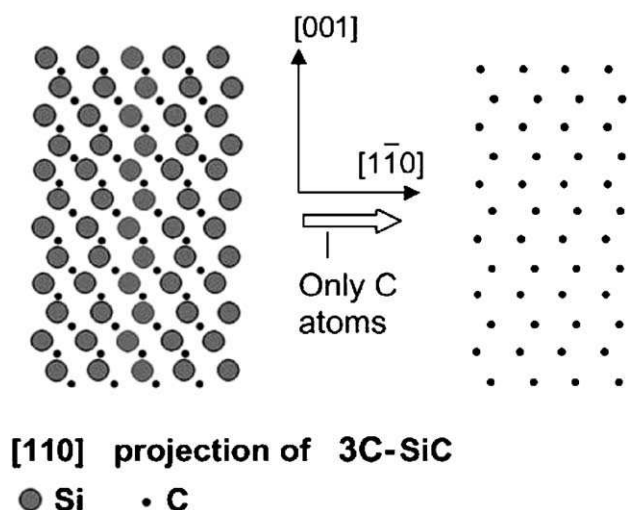
Fig. 2. Two-dimensional schematic showing a SiC lattice and positions of carbon atoms after silicon atoms have been removed from the lattice.

formed after silicon has been extracted from the SiC lattice. Bonding of remaining carbon atoms to each other by single or double bonds leads to formation of an amorphous porous network structure shown in Fig. 1a.

If treatment temperatures rise to 1000 °C, graphitization occurs. TEM studies confirm that longer treatment times and temperatures of 1000 °C and above lead to ordering of disordered carbons and ultimately to graphitization. This is an evolutionary process progressing with time over a range of temperatures. At first, amorphous carbon develops a lamellar network with graphitic bonding character. Small clusters of six membered rings create networks similar to the carbonization process described by Patrick [18]. Continuing heat treatment allows the formation of graphene sheets resembling turbostratic carbon. Lattice spacing in turbostratic carbon exceeds that of graphite.

Turbostratic carbon planes shown in the HRTEM image in Fig. 3a have a d_{002} spacing exceeding 0.35 nm. The schematic in Fig. 3b visualizes the enlarged interplanar spacing and imperfect graphenic lamellae. The correlation between the layers increases further developing the typical hexagonal honeycomb structure. The conversion process is completed by forming planar graphite sheets with an interplanar lattice parameter of 0.334 nm (Fig. 3c). Highest graphitization rates are observed in samples treated at 1000 °C and above, particularly in the powder sample 2, and may be assisted by gas phase transport or surface diffusion.

Constraint of surrounding carbon may lead to formation of ribbons (Fig. 4a) instead of a closed spherical configuration. The ribbon structures are similar to PAN-based carbon fibers as seen in the schematic in Fig. 4b. During transformation of hexagonal diamond structures, bent graphitic structures are formed. These so-called ribbons contain carbon with hexagonal graphene sheets and a lattice spacing of $d_{002} = 0.34$ nm. They are of short-range order with the orientation parallel to the c-axis. In contrast to sample 1, a higher graphitization degree is observed in sample 2 forming graphitic needles with graphitic walls ($d_{002} = 0.335$ nm) of short to medium range order (Fig. 5). The treatment times and temperatures of samples 2 and 4 are the same. However, CDC in sample 2 is produced using SiC powder and the higher surface area of the power allows higher reaction rates, resulting in a higher state of graphitic phase. The spiraling needle in Fig. 5b can be formed by scrolling graphene sheets and forming a sharp tip. A model of overlapping graphite sheets was reported earlier [19].

HRTEM studies on bulk CDC show the presence of carbon onions, curved graphitic shapes, tubular structures, nanotubes, and disordered or amorphous carbon. Larger quasi-spherical particles may transform to polyhedral particles with closed shells if annealing is continued [20].

The mechanism of the graphitization process at the interface between diamond and graphite has been described [14].
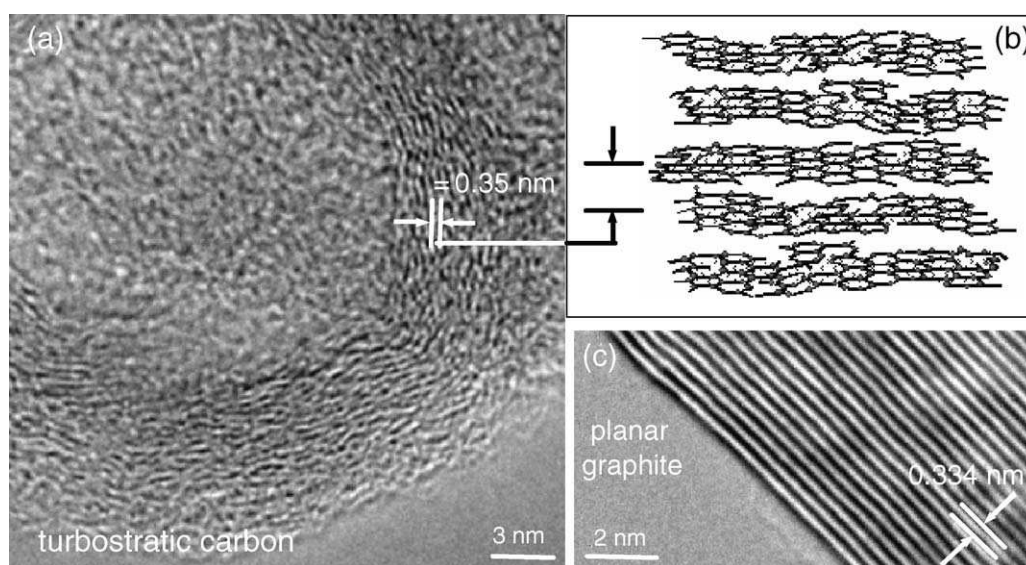

Fig. 3. (a) TEM image of turbostratic carbon surrounded by disordered carbon (sample 1, powder, 27 h at 600 °C). The schematic in (b) illustrates the structure of turbostratic carbon. The registry between the graphene layers emerges and lattice spacing of 0.35 nm is found. Higher treatment temperatures (sample 2, powder, 24 h at 1000 °C) lead to the formation of planar graphite with a lattice spacing of 0.334 nm observed in the outer CDC layer.
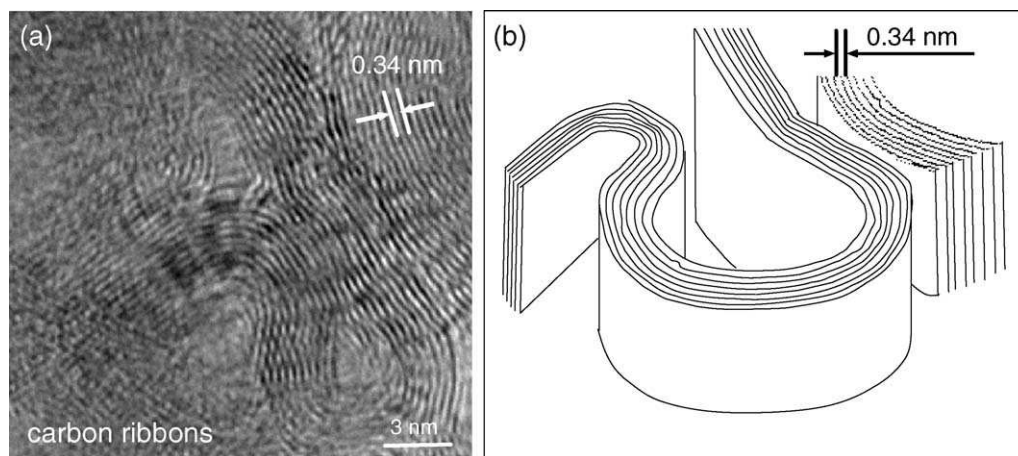
Fig. 4. (a) TEM image of carbon ribbons in sample 4. Lattice spacing of ribbons is 0.34 nm while the site correlation in the *c*-axis is lower than in graphite. The ribbons are stacked parallel to each other to form short-range carbon fiber similar to the PAN-fiber as can be seen in the schematic (b).

Fig. 6 shows an area of the phase transformation of nanocrystalline hexagonal diamond to carbon nanotubes. The inverse fast Fourier transformed (IFFT) TEM image in Fig. 6a shows a typical quasi-spherical diamond particle (dashed area at (a)) with a lattice spacing of 0.193 nm found at the interface. Bent graphitic planes are formed (marked by arrows in lower left side of the TEM image) which develop into fullerenic shells. Fig. 6b and c are IFFT images of growing nanotubes and spherical particles with one to three shells and a diameter of up to 2.3 nm indicated by arrows in Fig. 6b and c.

The phase transformation of diamond to graphite occurs by exfoliation of the preferential [1 0 0] diamond plane to graphite.

It is observed that three [1 0 0] diamond planes match up with two (0 0 0 1) planes of graphite while simultaneously minimizing the strain at the interface [14]. Other diamond planes, such as the (1 0 1) plane can also transform to graphitic planes. The phase transformation of nanocrystalline diamond to graphitic particles may introduce stress in the newly formed structure owing to the different densities of the carbon allotropes. This may be an explanation for why *d*-spacing values for dense carbon onions are decreased. Another reason for lower *d/n* values in onion structures may be the mixed sp^2–sp^3-bonding forcing interplanar compression of planes by linking graphitic shells by electron irradiation. However, EELS investigation could not
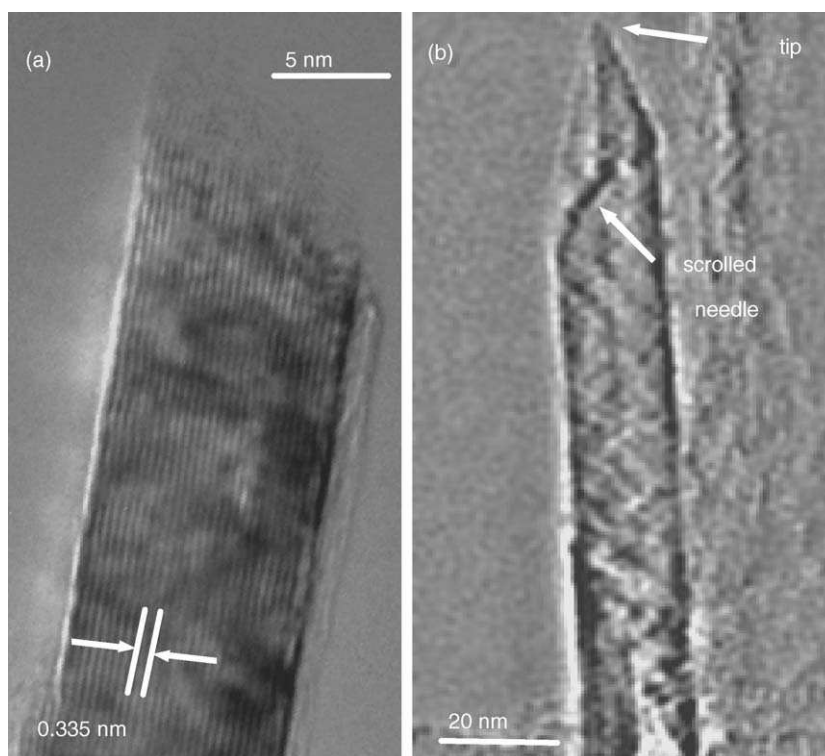

Fig. 5. TEM images of nanosized graphite needles observed in sample 2. The TEM image in (a) shows a graphite needle or plate with a broken tip. The graphite sheets scroll forming a sharp tip in (b).
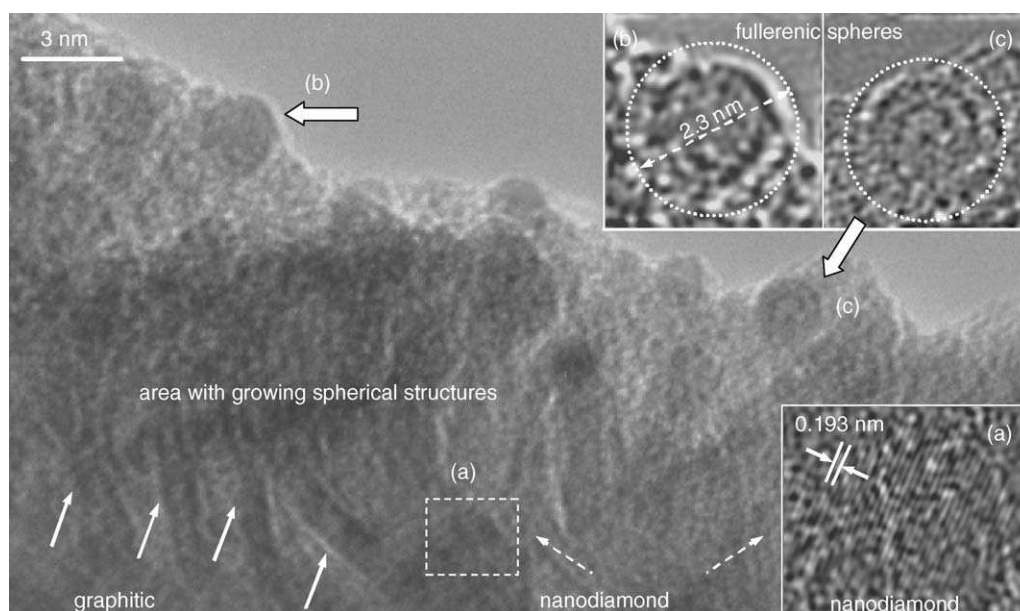
Fig. 6. TEM images identify locations of nanocrystalline, hexagonal diamond clusters (IFFT image in (a)). While diamond transforms to graphite, fullerenic structures may also be formed. IFFT images in (b) and (c) identify single and double walled tubes or shells with the outer diameter of 2.3 nm (sample 4).

support this hypothesis. Lattice spacing of 0.275 nm of newly formed, curved graphite planes decreases to ∼18% less than the standard d/n value for graphite (0.335 nm). The diamond nanocrystals transform to graphite and the formation of carbon onions is very likely [14,21]. After the initial exfoliation of the diamond surface, arrangement of spherical shells around the nanocrystalline diamond core occurs. At this stage, the shells are not perfectly formed yet and contain many defects. Though, as the process continues until the residual diamond phase in the core transforms, a carbon onion, nanotube or ribbon is formed. The planes of the final spherical onion structure appear to exhibit a smoother curvature than the transitional states. The core of final developed carbon onions has been observed to be either hollow or dense. Lattice spacing values for hollow onion structures in the interior of the structure do not change in comparison to the outer shells of the onion and have the lattice spacing of graphite. However, the lattice spacing for more common, dense onion structures decreases towards the center of the structure in comparison to the values of the outer shells because stress relaxation cannot occur in these onions. Illustrating this fact in numbers, lattice spacing was decreasing from 0.334 nm in outer onion shells to 0.275 nm in the inner shell. The latter value is close to the values observed at the diamond/graphite interface and it roughly corresponds to graphite compressed to the volume of diamond. The schematic in Fig. 7 illustrates a possible formation mechanism of dense and hollow carbon onions. In the case of dense onions, it is assumed the initial structure is a nearly spherical diamond structure with a diameter of up to 5 nm. The phase transformation process initiates at the lowest energy points of the structure (depicted by the arrows at step 1 in Fig. 7), at the "corners". It can be expected that the exfoliation process is established simultaneously and the bonding character changes at the corners and graphitic units are formed (step 2). During the next step, the units of different corners connect and close a uni-

form graphitic sphere around the remaining diamond core. The diamond core will be transformed forming a dense onion structure with enormous pressure in the core owing to the difference in density of graphite and diamond. The reverse process, the transformation of carbon onions to diamond by irradiating with an electron beam has been demonstrated [22] and is expected to take place for CDC derived dense carbon onions as well. On the right in Fig. 7, the formation of a hollow onion structure is illustrated. In this case, it is assumed that the basic structure is a non-equiaxial diamond structure rather than the for CDC typical circular nanodiamonds. Again, the "weakest" points of the structure will transform at first to graphite, which are the edges. However, closing the graphite ring will be postponed owing to the non-circular basic structure. This effect gives opportunity to relax the core as indicated by the direction of the arrows in step 3. As the atoms rearrange driven by achieving the most advantageous energy state, the graphite ring completes while arising a hollow core. The final onion structure is pressure-less. Hollow onions are observed infrequently, which is in confirmation with the fact that the observed nanodiamonds are most often of spherical nature. Fig. 8(left) shows a statistical computed diagram illustrating the lattice spacing versus the distance of the lattices from the core of the onion for three characteristic onion structures found in CDC. All three types of onion structures appear circular in TEM. Onions 2 and 3 have a dense core in contrast onion 1, which is hollow. The more common dense onion structures have a similar appearance but differ in size. As can be seen in the dense onion structure of Fig. 8(right), the lattice parameter increases if measured from the core of the onion toward the surface shells of the structure. The interplanar spacing at the surface is close to the typical graphite values (0.33 nm) while the inner layers are compressed with spacing of 0.27 nm. It is also observed that lattice spacing for the outer shell may exceed typical graphite values (see diagram), which may be caused
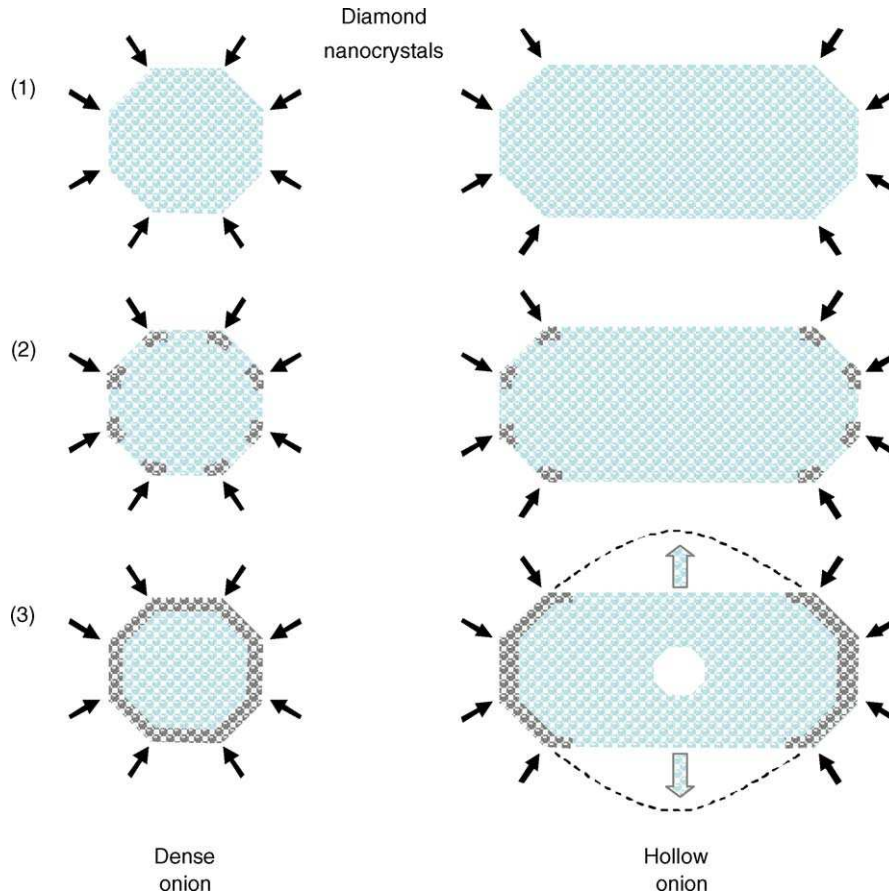
Fig. 7. Schematic showing a possible formation mechanism of dense and hollow carbon onions from nanosized diamond crystals.

by not fully closed outer shells or disordered surface of the shell.

Dense carbon onions are multi-walled fullerenes. The bulk modulus B_0 for C_{60} molecules is calculated to be 843 GPa [23] while B_0 for diamond is 441 GPa [24]. Since the dense onions structures produced by CDC indicate high stresses in the core, it is of interest to estimate stress, pressure and the bulk modulus. As reported for planar graphite, a pressure of 36.5 GPa is necessary to compress lattice spacing along the *c*-axis from 0.33 to 0.27 nm [25]. The stress, the pressure and the bulk modulus in dense carbon onions in CDC were estimated combining the elasticity theory with experimental data [25–28]. As a result, we obtained $B_{0\,shell} = 57$ GPa for outer shells with a lattice spacing of 0.335 nm. This value exceeds the bulk modulus for hexagonal planar graphite (34 GPa) [27]. If the particle is regarded as an elastic continuum under hydrostatic pressure, which is expected in the center of the onion, the pressure is universally equal and we obtain for the core of the onion $B_{0\,core} = 172$ GPa. In similar to studies on planar graphite, the volume decreased with pressure due to smaller distances of the graphite layers while the bulk modulus rose from 34 to 42.9 GPa. In comparison with other carbon structures, the bulk modulus in CDC-onions
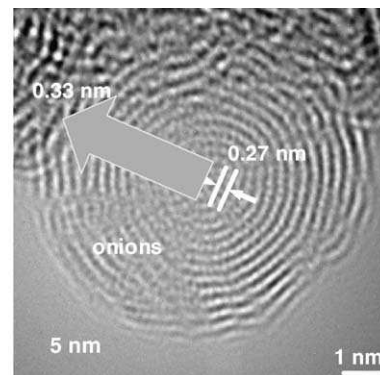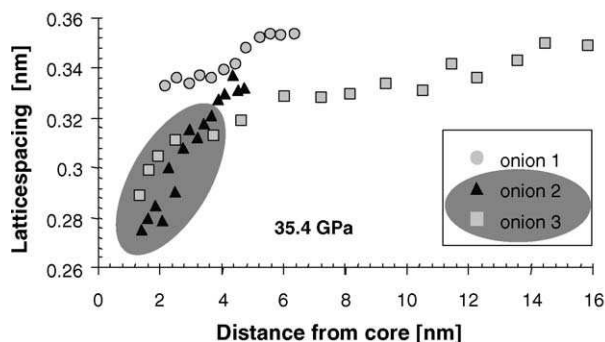

Fig. 8. Plot showing the compression of the lattice vs. the distance from the core of the onion. The TEM image shows a high-pressure onion cell with a lattice parameter changing from the core to the outer shells of the structure.
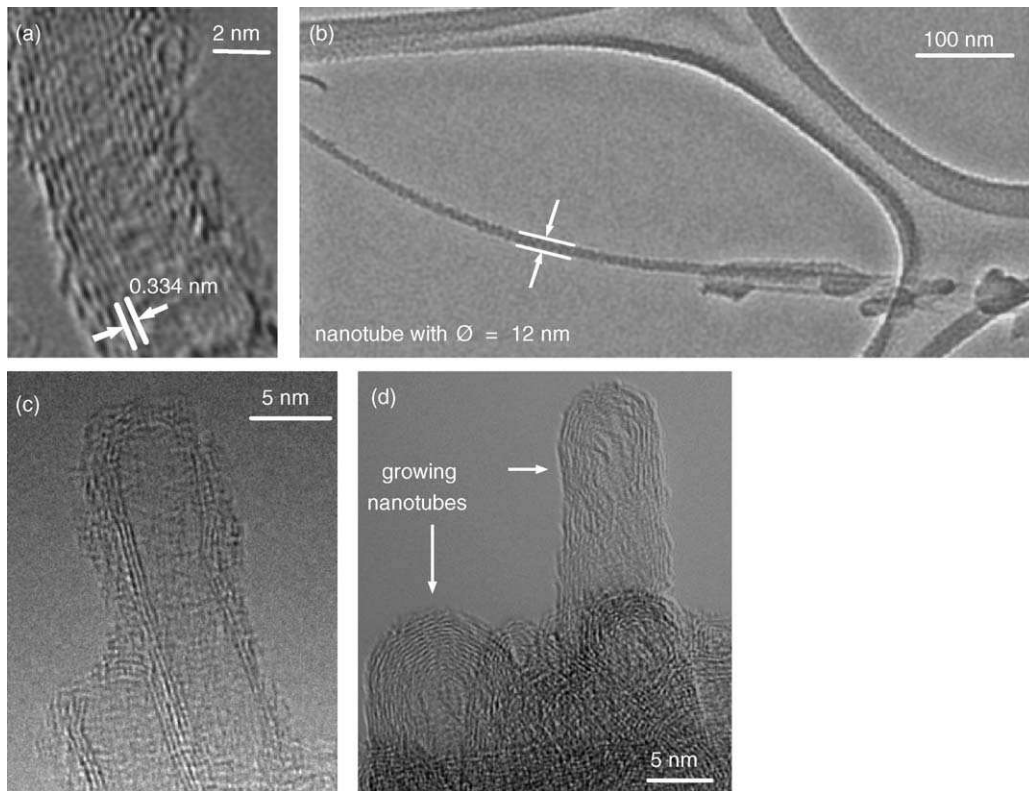
Fig. 9. TEM images of nanotubular structures formed at 1000 °C in Cl$_2$–H$_2$ gas mixtures during CDC process. (a) MWNT with disordered layers on the surface and an interplanar spacing of 0.334 nm in the inner tube (sample 3). (b) Tubes grow up to 1 μm in length with diameter of up to 12 nm in sample 3. (c) Triple-walled nanotubes in sample 4. (d) MWNTs in sample 5.

exceeds values for graphite and carbon nanotubes in a bundle [27,29].

To confirm that virtually all elemental forms of carbon can be synthesized by the CDC process, tubular structures have been observed using TEM. Carbon nanotubes (CNT) have been first discovered by Iijima [30] and previously produced by catalytic pyrolisis of hydrocarbons [31–33], carbon-arc discharge techniques [34] and condensed-phase electrolysis [35]. Much experimental work has been done on multi-wall carbon nanotubes. By rolling up a single layer of an sp^2-bonded graphene sheet (honeycomb structure) as a cylinder and capping each end of the cylinder with half of a fullerene molecule, a one layer "fullerene-derived" tubular structure is formed [36]. The nanotubular structures found in this work grow with no preferential orientation with respect to the surface. In addition to small-diameter nanotubes (Fig. 9a), larger multi-walled nano tubes (MWNT) were observed (Fig. 9d). The outer walls of the MWNTs appear to be parallel. Interplanar spacing for the graphitic walls is found to be close to that of ordered graphite whereas the outer walls at the surface show occasional imperfections and decreased lattice spacing (Fig. 9a and c). MWNTs may grow up to 1 μm in length with a diameter of about 12 nm (Fig. 9b). Fig. 9d shows ordered MWNTs with diameters ranging from 7 to 10 nm. Overall, the diameter of the tubes varies from 6 to 13 nm. The tubes are closed in most cases even those with disordered outer walls. Nearly spherical hollow carbon onions and polyhedral, hollow, multi-walled carbon structures (Fig. 10) are

often found along with MWNTs. This suggests a common mechanism for growth of onions and nanotubes. Polyhedral structures are hollow and vary in appearance regarding the number of corners, size and number of shells. The number of graphite layers in the walls varies from 2 to 20 with a constant lattice parameter of 0.334 nm for adjacent layers. The particles seem to be ordered. Several polyhedra may also be attached to each other. Some of these structures in fact may be tubular yet observed parallel to its tube axis marked by arrows in Fig. 10b.

The formation of polyhedral structures may be a result of the phase transformation of bigger diamond nanocrystals. In this case, polyhedrals transform to spherical closed shell onions if enough energy is provided [20]. Graphitic shell curling and closure at nanoscale under the thermal conditions provided may be due to the difference in surface energy of the basal plane (0.135 J/m^2) and the planes formed by the edges of the basal planes, namely (1 0 1) and (1 1 2) (about 4.8 J/m^2) [37].

Formation of the polygonal outer shell on a cylindrical nanotube can be seen in the lower left part of Fig. 10b. Thus, nanotubes and polyhedral particles may be the result of graphitization of diamond and amorphous carbon in the outer layer of the CDC film. Similar structures were formed as a result of graphitization of the surface of large diamond crystals [20]. It is important to mention that closed fullerenic structures are formed at 1000 °C due to presence of pentagonal rings and defects. Similar structures were produced by chlorination of Al$_4$C$_3$ [38] and also found in amorphous carbon produced by conventional
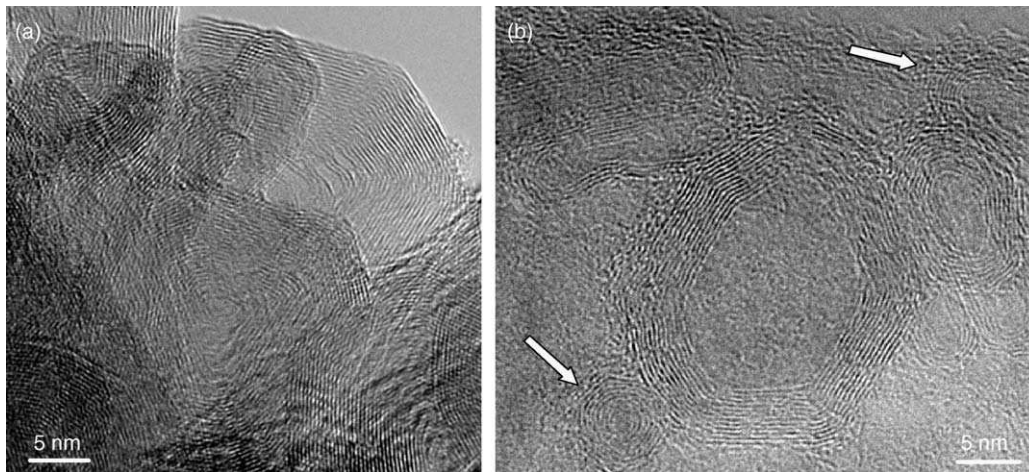
Fig. 10. Typical HRTEM images of multi-shell polyhedral structures found in CDC (a) and polyhedral carbon nanotubes (b) found in sample 5.

methods [16]. However, since formation of tubular structures was not observed uniformly, it is possible that nanotube growth was catalyzed by small amounts of metal impurities present in commercial carbide samples.

3.2. Diamond structures

SiC/CDC interface studies confirm the presence of sp³-bonded carbon. Coatings produced with high hydrogen contents in the gas mixture contain some diamond, mainly lonsdaleite and a smaller amount of cubic, 3C, diamond.

TEM imaging of cubic diamond shows characteristic lattice parameter of 0.206 nm. The cubic diamonds are between 2 and 5 nm in diameter and often surrounded with amorphous carbon. The HRTEM image in Fig. 11a and the corresponding CBED pattern in the inset show cubic diamond. The CBED was taken from the nanocrystalline area. Lattice spacing seen in the pattern is 0.206 nm for the (1 1 1) direction and the (2 2 0) direction was computed as 0.126 nm. The obtained lattice spacing is characteristic for cubic diamond (JCPDS 6-0675) as seen in Table 2.

However, the predominant diamond structure synthesized is lonsdaleite. These nanodiamonds have random orientation and are often embedded in amorphous carbon. The HRTEM image in

Fig. 11b shows typical nanocrystals in sizes of 2–5 nm (sample 4). CBED and SAED verify 2H diamond with the lattice spacing being in agreement with the values reported in JCPDS 19-0268.

In addition, electron diffraction studies indicate the formation of diamond polytypes. Lattice spacing calculated using CBED pattern is very close to that of the 4H hexagonal polytype (Table 3). A typical SAED recorded from a polycrystalline diamond film is shown in Fig. 12a. Reflections are visible up to (2 0 6) planes showing a 0.085 nm lattice parameter and include the typical reflection for the (1 0 3) plane in 4H diamond at 0.171 nm. This reflection is also observed in CBED as can be seen in Fig. 12b taken from the nanocrystalline particle shown in Fig. 12d. A ring of excess HOLZ lines around the inner CBED reflections is due to a small convergence semi-angle. The 4H structure has an ABCB/ABCB··· stacking order as illustrated in the schematic (Fig. 12c). Higher order polytypes hold very close ground-state energies. 4H was found to be energetically most favorable followed by 6H and 8H [39].

Fig. 13a shows another diamond polytype. The FFT image in the inset illustrates the crystallinity of the area and different phases can be identified. SAED pattern taken from nanocrystalline diamond films frequently show forbidden reflections for 3C and 2H diamond at 0.178 nm. A distinctive SAED can be
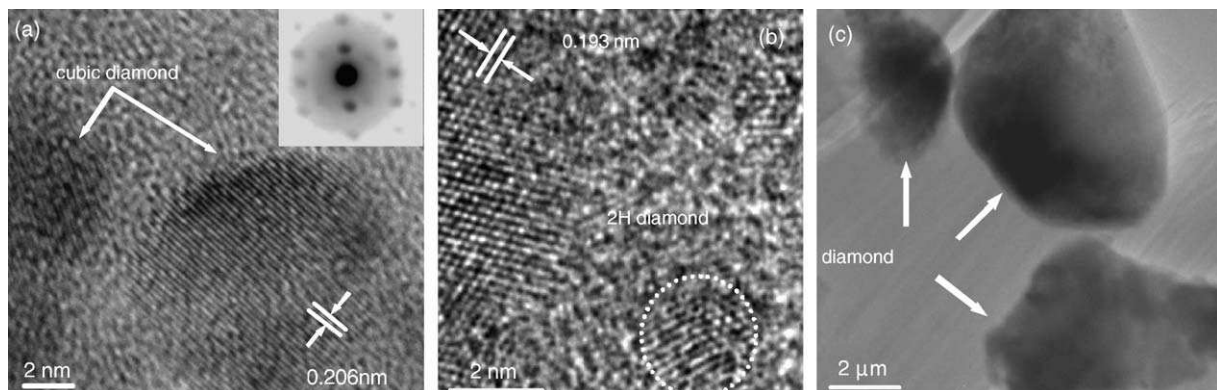

Fig. 11. TEM images of diamond structures in CDC. (a) Near spherical cubic nanodiamond ($d_{1 1 1} = 0.206$ nm) and its CBED. (b) Hexagonal, 2H, nanostructured diamond (lonsdaleite). (c) Microcrystals grow up to 800 nm in sample 4.

Table 2
Experimental *d*-spacing in (nm) of n-diamond compared to standard JCPDS data of cubic diamond and lonsdaleite

Experiment (*d*-spacing)	n-Diamond		Cubic diamond, *Fd3m*		Lonsdaleite, *P6₃/mmc*	
	hkl	*d*-Spacing	*hkl*	*d*-Spacing	*hkl*	*d*-Spacing
					1 0 0	0.219
0.218	1 1 1	0.206	1 1 1		0 0 2	0.206
0.206				0.206	1 0 1	0.193
0.192	2 0 0[a]	0.178				
0.178					1 0 2	0.150
0.150	2 2 0	0.126	2 2 0		1 1 0	0.126
0.126				0.126	1 0 3	0.116
0.117					0 2 0	0.1092
0.110	3 1 1	0.107	3 1 1		1 1 2	0.1075

[a] Indicates a forbidden cubic diamond reflection (2 0 0), which was observed for n-diamond and is charcteristic of this phase.

seen in the inset of Fig. 13a showing sharp Bragg reflections up to the order of (8 0 0), indicating good crystallinity. This carbon structure can be interpreted as so-called n-diamond (or γ-carbon) [12]. Nanocrystalline n-diamond structures nucleate and grow similar to hexagonal diamond structures and have a size of about 2–5 nm in diameter. They form at the SiC/CDC interface and are embedded in disordered carbon structures. Similar to hexagonal and cubic diamond, n-diamond was found to form larger microcrystals. Larger diamond crystals have been infrequently observed measuring of up to 800 nm (hydrogen was present in the gas mixture, Fig. 11c). The growth of microcrystalline diamond may be explained via gas phase transport reactions in the nanoporous CDC layer as described in Welz et al. [14] SAED pattern drew first attention to this structure because they showed strong forbidden reflections. Reflections of (2 0 0), (2 2 2) and (4 2 0) were consistently observed, which is not unusual for cubic diamond due to possible double or multiple reflections (inset in Fig. 13b). But they were stronger than expected from
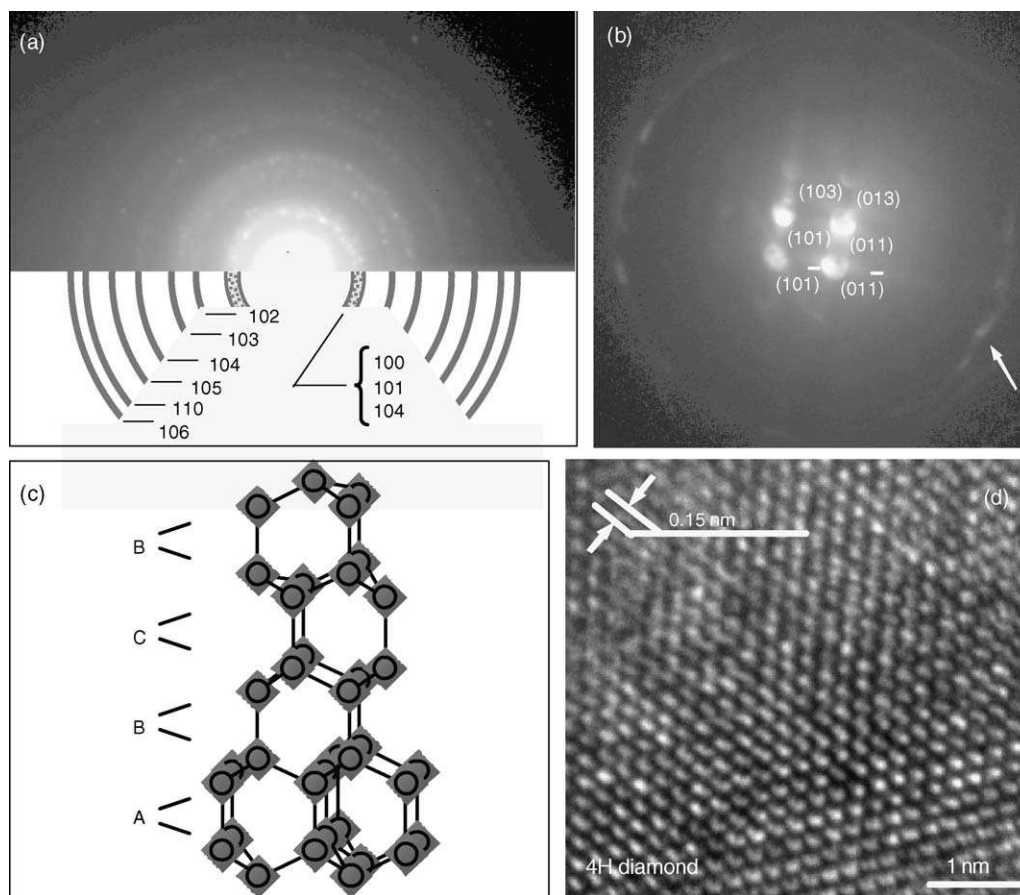

Fig. 12. Diamond polytypes (a) SAED of a polycrystalline diamond area. (b) CBED pattern with indexed reflections of a 4H diamond crystal. HOLZ reflections marked by the arrow appear around the inner reflections. (c) The stacking order of 4H diamond ABCB/ABCB··· is illustrated in the schematic. (d) HRTEM image of a 4H diamond nanocrystal with $d_{104} = 0.149$ nm (sample 4).
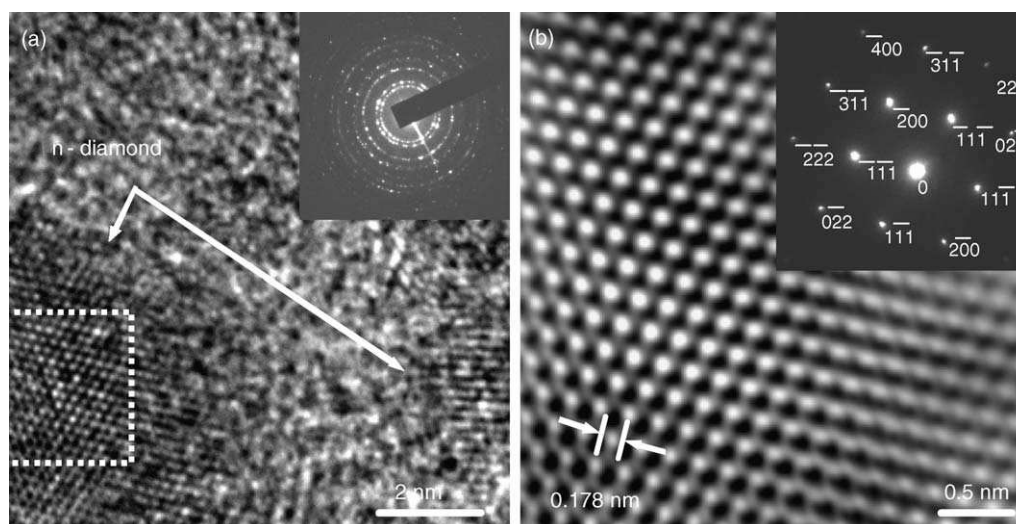
Fig. 13. (a) HRTEM image of nanocrystalline n-diamond embedded in amorphous carbon. The SAED in the inset shows good crystallinity with sharp Bragg reflections up to the order of (8 0 0). The framed diamond crystal in (a) is magnified in (b) using IFFT. Lattice parameter and reflections are comparable to cubic diamond. The image in (b) shows the lattice parameter of $d_{200} = 0.178$ nm which is characteristic for n-diamond. The distinctive reflection (2 0 0) in the SAED is forbidden in cubic diamond.

Table 3
Experimental *d*-spacing in (nm) of 4H diamond in comparison to standard JCPDS data

Experiment	hkl	JCPDS 26-1078
0.218	1 0 0	0.21842
0.211	1 0 1	0.21112
0.206	0 0 4	0.20593
0.193	1 0 2	0.19296
0.171	1 0 3	0.17093
0.149	1 0 4	0.14983
0.131	1 0 5	0.13153
0.126	1 1 0	0.12610
0.116	1 0 6	0.11623

multiple diffraction excluding this possibility. The appearance of the (2 0 0), (2 2 2) and (4 2 0) reflections may be interpreted as a loss of the diamond-glide plane, which would result in a lowering of the symmetry from $Fd3m$ to $F\bar{4}3m$. Formation of n-diamond has been reported in CVD synthesis on Si substrates [13]. The mechanisms of n-diamond formation in CVD may be similar to that in the CDC process. Moreover, since n-diamond was formed at the Si/diamond interfaces only [13], Si doping may be responsible for its formation.

The *d*-spacing values and the crystallographic appearance in diffraction pattern of the n-diamond polytype synthesized in our experiments are in agreement with values reported in JCPDS 43-1104. Characteristic values for the (2 0 0) plane are found to be 0.178 nm (Fig. 13b and Table 2).

4. Discussion

TEM studies identified sp^2-bonded carbon as well as some sp^3-bonded carbon in samples under study. A mixture of carbon structures is formed upon chlorination. The formation of turbostratic graphite and amorphous carbons was observed in all samples under study. Similar structures have been observed in carbons produced by decomposition of organic precursors [16]. Ar–Cl$_2$ gas mixture treatments favor the formation of graphite at longer treatment times and 1000 °C or above. The graphitization degree within the CDC film increases from the SiC/CDC interface toward the coating surface. This fact has not been detected by Raman spectroscopy [40] but was observed during TEM experiments. Graphitization may lead to shrinkage, cracking and spallation of the CDC layer. After formation of carbon onions, polyhedral and ribbon type structures, graphitization will require solid state diffusion of carbon, which can only be achieved at temperatures close to 3000 °C. Tubular and polyhedral structures are mainly found in samples with hydrogen added to the gas mixture and at treatment temperatures of 1000 °C. The cause may be increased surface diffusion of carbon assisted by hydrogen. Simultaneously, satisfying the dangling bonds of immediate "surface" carbon atoms with hydrogen hinders the formation of graphitic sp^2 or carbynic sp structures [41]. Hydrogen added to the Ar/Cl$_2$ gas mixture promotes the nucleation of nanocrystalline diamond and its further growth. Predictions by several groups confirm that diamond at nanoscale may be more stable than graphite because of its lower surface energy compared to graphite. According to Gamarnik, diamond is the stable phase of carbon up to a crystal size of 5 nm at temperatures not exceeding 1200 °C [42]. These theoretical predictions are in agreement with our experimental observations [14]. Hexagonal diamond, which appears to be the main sp^3-bonded diamond structure, is similar to 6H-SiC. There may be a link between the diamond structures formed and the 6H-SiC used as a precursor, but this hypothesis needs experimental verification. Although various carbon structures have been synthesized simultaneously, their content can be manipulated by varying temperature, gas composition and the structure of the metal carbide. EEL spectra (Fig. 14a) identify the change of bonding character in carbon structures in CDC. Carbon K-edges
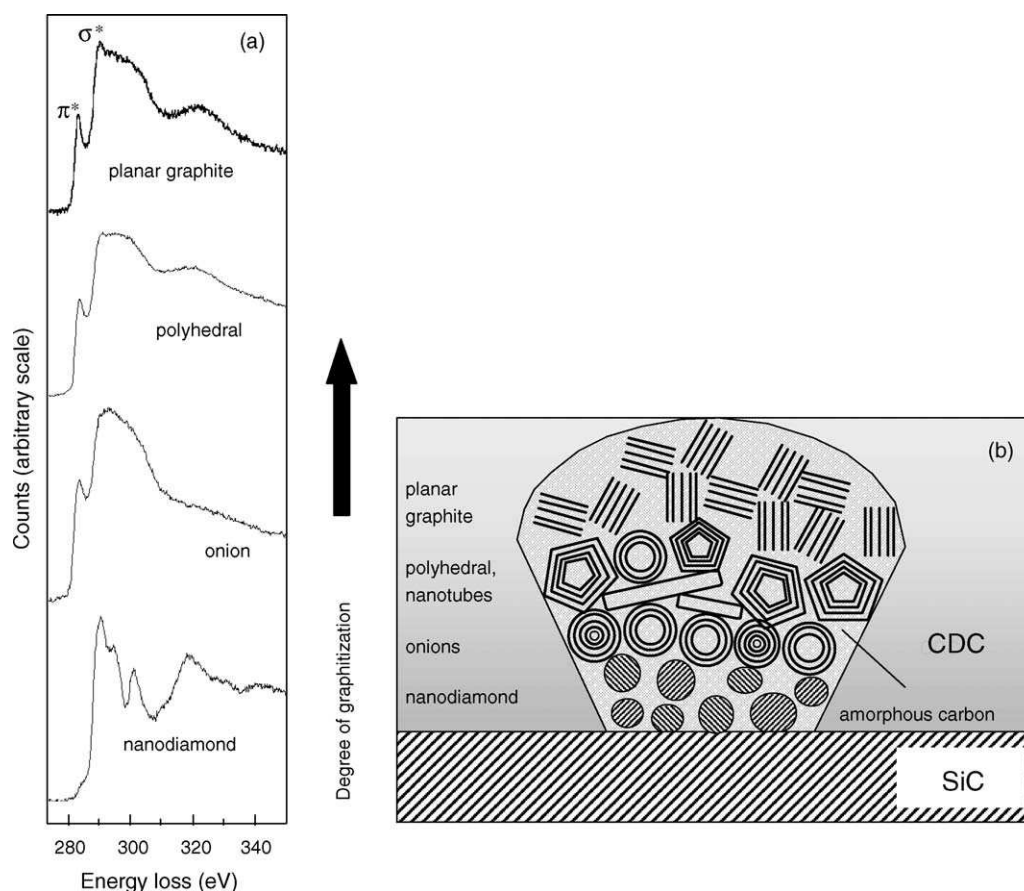
Fig. 14. Electron energy loss spectra taken from typical carbon structures in samples 2 through 5 (a) and a schematic of structural changes in the CDC film (b).

after background subtraction expose peaks at 285 eV (π^*-peak) and at 290 eV (σ^*-peak). Among the four structures shown in Fig. 14a (nanocrystalline diamond, a dense carbon onion, polyhedral carbon and planar graphite), a variation in the π^*- and σ^*-peak intensities is observed. The nanodiamond crystal shows evidence of sp³-bonding. However, the little hump at 285 eV indicates sp²-bonding, which may be due to surrounding amorphous carbon. Bonding character changes with the formation of carbon onions. Despite strong lattice plane compression, sp²-bonding is observed. Graphitization continues by forming polyhedral structures and is complete after forming highly oriented, planar graphite crystals.

5. Summary and conclusions

A wide variety of carbon structures have been observed in CDC samples. The structure of CDC depends on the processing conditions. Turbostratic and amorphous carbons, spherical, polyhedral and tubular structures, graphite or diamond can be present in CDC depending on process parameters and location within the CDC film.

Films grown at 600 °C in chlorine are predominantly porous and amorphous. Planar graphite appears along with randomly oriented carbon whiskers and ribbons in samples treated in chlorine at 1000 °C.

Phases found close to the SiC/CDC interface include nanocrystalline sp³-bonded hexagonal and cubic diamond. Microcrystalline diamond growth was primarily observed when hydrogen was added stabilizing the dangling carbon bonds.

As a result of the diamond/graphite transformation, carbon onions with dense or hollow cores and nanotubes are formed. They vary in size, length and number of lattice walls. Longer treatment favors polygonization. The structural changes in CDC films containing various carbon structures are illustrated in Fig. 14b.

Acknowledgements

References

[1] Y. Gogotsi, S. Welz, D.A. Ersoy, M.J. McNallan, Conversion of silicon carbide to crystalline diamond-structured carbon at ambient pressure, Nature 411 (2001) 283.

[2] Y. Gogotsi, I.D. Jeon, M.J. McNallan, Carbon coatings on silicon carbide by reaction with chlorine-containing gases, J. Mater. Chem. 7 (1997) 1841–1848.

[3] M.S. Dresselhaus, Future directions in carbon science, Ann. Rev. Mater. Sci. 27 (1997) 1–34.

[4] H. Morkoc, Large-band-gap SiC, III–V nitride, and II–VI ZnSe-based semiconductor device technologies, J. Appl. Phys. 76 (1994) 1363–1398.

[5] A.W. Phelps, W. Howard, D.K. Smith, Space groups of the diamond polytypes, J. Mater. Res. 8 (1993) 2835–2839.

[6] K.E. Spear, A.W. Phelps, W.B. White, Diamond polytypes and their vibrational spectra, J. Mater. Res. 5 (1990) 2277.

[7] M. Frenklach, R. Kematick, D. Huang, W. Howard, K.E. Spear, A.W. Phelps, R. Koba, Homogeneous nucleation of diamond powder in the gas phase, J. Appl. Phys. 66 (1989) 395.

[8] A.K. Sharma, R.D. Vispute, D.S. Joag, S.B. Ogale, S.D. Joag, P. Ayyub, M. Multani, G.K. Dey, S. Banerje, Diamond nucleation at the organic liquid–metal interface by laser induced reactive quenching, Mater. Lett. 17 (1993) 42.

[9] R. Kapil, B.R. Mehta, V.D. Vankar, Growth of 8H polytype of diamond using cyclic growth/etch oxy-acetylene flame setup, Thin Solid Films 312 (1998) 106–110.

[10] Y. Lifshitz, X.F. Duan, N.G. Shang, Q. Li, L. Wan, I. Bello, S.T. Lee, Nanostructure: epitaxial diamond polytypes on silicon, Nature 412 (2001) 404.

[11] R. Kapil, B.R. Mehta, V.D. Vankar, Synthesis of 15R polytype of diamond in oxy-acetylene flame grown diamond thin films, Appl. Phys. Lett. 68 (1996) 2520.

[12] H. Hirai, K.I. Kondo, Modified phases of diamond formed under shock compression and rapid quenching, Science 253 (1991) 772–774.

[13] M. Rossi, G. Vitali, M.L. Terranova, V. Sessa, Experimental evidence of different crystalline forms in chemical vapour deposited diamond films, Appl. Phys. Lett. 63 (1993) 2765–2767.

[14] S. Welz, Y. Gogotsi, N. McNallan, Nucleation, growth and graphitization of diamond nanocrystals during chlorination of carbides, J. Appl. Phys. 93 (2003) 4207.

[15] Y. Gogotsi, A. Nikitin, H. Ye, W. Zhou, J.E. Fischer, B. Yi, H.C. Foley, M.W. Barsoum, Nanoporous carbide-derived carbon with tunable pore size, Nat. Mater. 2 (2003) 591–594.

[16] P.J.F. Harris, A. Burian, S. Duber, High-resolution electron microscopy of a microporous carbon, Phil. Mag. Lett. 80 (2000) 381–386.

[17] P.J.F. Harris, S.C. Tsang, High-resolution electron microscopy studies of non-graphitizing carbons, Phil. Mag. A 76 (1997) 667–677.

[18] J.W. Patrick, Porosity in Carbons, British Library Cataloguing in Publication Data, London, 1995.

[19] R. Bacon, Growth, structure, and properties of graphite whiskers, J. Appl. Phys. 31 (1960) 283–290.

[20] V.L. Kuznetsov, A.L. Chuvilin, Y.V. Butenko, I.Y. Mal'kov, V.M. Titov, Onion-like carbon from ultra-disperse diamond, Chem. Phys. Lett. 222 (1994) 343–348.

[21] V.L. Kuznetsov, I.L. Zillerberg, Y.V. Butenko, A.L. Chuvilin, Theoretical study of the formation of closed curved graphite-like structures during annealing of diamond surface, J. Appl. Phys. 86 (1999) 863–870.

[22] P. Wesolowski, Y. Lyutovich, F. Banhart, H.D. Carstanjen, H. Kronmuller, Formation of diamond in carbon onions under MeV ion irradiation, Appl. Phys. Lett. 71 (1997) 1948–1950.

[23] R.S. Ruoff, A.L. Ruoff, Is C_{60} stiffer than diamond? Nature 350 (1991) 663–664.

[24] H.J. McSkimmin, W.L. Bond, Elastic moduli of diamond, Phys. Rev. 105 (1957) 116–121.

[25] R.W. Lynch, H.G. Drickamer, Effect of high pressure on the lattice parameters of diamond, graphite, and hexagonal boron nitride, J. Chem. Phys. 44 (1965) 181–184.

[26] R.S. Ruoff, A.L. Ruoff, The bulk modulus of C_{60} molecules and crystals: a molecular mechanics approach, Appl. Phys. Lett. 59 (1991) 1553–1555.

[27] B.T. Kelly (Ed.), Physics of Graphite, vol. 74, Applied Science Publishers, Englewood, NJ, 1981.

[28] C.S. Barrett, T.B. Massalski, Structure of Metals, McGraw-Hill Book Co., New York, NY, 1966.

[29] S. Reich, C. Thomsen, Elastic properties of carbon nanotubes under hydrostatic pressure, Phys. Rev. B 65 (2002) 153401–153407.

[30] S. Iijima, Helical microtubes of graphitic carbon, Nature 354 (1991) 56–58.

[31] S. Amelinckx, X.B. Zhang, D. Bernaerts, X.F. Zhang, V. Ivanov, J.B. Nagy, A formation mechanism for catalytically grown helix-shaped graphite nanotubes, Science 265 (1994) 635.

[32] M. Endo, K. Takeuchi, K. Kobori, T. Takahashi, H.W. Kroto, A. Sarkar, Pyrolytic carbon nanotubes from vapor-grown carbon fibers, Carbon 33 (1995) 873.

[33] J. Libera, Y. Gogotsi, Hydrothermal synthesis of graphite tubes using Ni catalyst, Carbon 39 (2001) 1307–1318.

[34] T.W. Ebbesen, P.M. Ajayan, Large-scale synthesis of carbon nanotubes, Nature 348 (1992) 220.

[35] W.K. Hsu, J.P. Hare, M. Terrons, H.W. Kroto, D.R.M. Walton, P.J.F. Harris, Condensed-phase nanotubes, Nature 377 (1995) 687.

[36] M.S. Dresselhaus, G. Dresselhaus, R. Saito, Physics of carbon nanotubes, Carbon 33 (1995) 883–891.

[37] J. Abrahamson, The surface energies of graphite, Carbon 11 (1973) 337–362.

[38] J. Leis, A. Perkson, M. Arulepp, M. Kaarik, G. Svensson, Carbon nanostructures produced by chlorinating aluminium carbide, Carbon 39 (2001) 2043–2048.

[39] H.G. Salunke, A.K. Sharma, G.P. Das, P. Ayyub, Electronic structure of the 4H polytype of diamond, J. Phys.: Condens. Matter 8 (1996) 5801–5809.

[40] D.A. Ersoy, M.J. McNallan, Y. Gogotsi, Carbon coatings produced by high temperature chlorination of silicon carbide ceramics, Mater. Res. Innovat. 5 (2001) 55–62.

[41] B.V. Spitsyn, Handbook of Crystal Growth, Elsevier, 1994, p. 401–456.

[42] M.Y. Gamarnik, Energetical preference of diamond nanoparticles, Phys. Rev. B 54 (1996) 2150–2156.